Analele Universităţii de Vest din Timişoara
Vol. XLVI, 2005
Seria Fizică

IRON/IRON CARBIDES/CARBON CORE-SHELL NANOSTRUCTURES SYNTHESIZED BY LASER PYROLYSIS[1]

V. Ciupina[a], G. Prodan[a], F. Dumitrache[b], I. Morjan[b], R. Alexandrescu[b], E. Popovici[b], I. Soare[b], L. Albu[b], R. Birjega[b], B. David[c], O. Schneeweiss[c]

[a] *"Ovidius" University of Constanta, 124 Mamaia Bd., P.O.B. 900527 Constanta, Romania*

[b] *National Institute for Lasers, Plasma and Radiation Physics, Laser Department, P.O.Box MG-36, R-76900 Bucharest, Romania*

[c] *Institute of Physics of Materials, AS CR, Brno, Czech Republic*

Abstract
Multiphase composite nanoparticles presenting core-shell structures have been investigated by performing a detailed correlation between their synthesis parameters and the structural and magnetic properties. Basically in all the experiments iron pentacarbonyl as iron precursor and ethylene as laser energy transfer agent and as a secondary carbon source have been used. The capability of the synthesis technique to form nanocomposite particles by varying laser power density, inlet geometry, pressure in reactor chamberand gas precursors ratio was tested. The results proved that the laser pyrolysis can produce particles between 4 and 10 nm diameters. Their size may vary according to the reactor pressure and gas flows but their size distribution remain sharp as long as an optimized geometry of the reactor is used. As a second step, the structure and magnetic properties were studied by different techniques such as TEM, HREM, SAED, XRD, FT-IR and Raman spectroscopy. The investigations reveal that, depending on the input parameters, some samples exibit a nanocomposite structure consisting of iron/iron carbides (Fe_3C or Fe_2C_5) core wrapped in a shell of amorphous or turbostratic carbon. The different magnetic phase identification was performed using Mössbauer spectroscopy and thermo-magnetic analysis.
Keywords: iron-carbon nanocomposites ; iron carbides ; laser pyrolysis ; TEM.

1. Introduction

The nanoscale iron carbon materials are a new class of materials that has lately attracted much attention [1, 2]. Carbon, iron and their combinations have a large number of applications. An exemple is the magnetization size effects: below a critical size the iron based nanoparticles comprise just single-domains, then become superparamagnetic or have quantum tunnelling magnetization effect [3]. The embedding of metal-based nanoparticles in carbon

[1] Invited lecture presented to TIM-05 conference, 24-25 November, 2005, Timisoara

shell preserves and multiplies the magnetic features for a single nanoparticle and instates inertness to external detrimental conditions [4]. During the last year different synthesis methods were proposed for obtaining iron based nanostructures: gamma and alpha iron [5, 6], iron oxides [7, 8] and iron carbides [9, 10] phases.

In the recent studies we have reported the preparation of carbon encapsulated iron nanoparticlcs and their role as catalyst for carbon nanotubes and nanofibres [11, 12]. Also we have demonstrated the feasibility or this highly efficient laser technique for obtaining Fc-C nano-composite materials.

We present results about the synthesis of iron/iron carbides nano-cores embedded in carbon layers via a single-step copyrolysis method in which the continuous wave CO_2 laser beam irradiates a reactive gases mixture of iron pentacarbonyl vapors, ethylene and acetylene. Iron pentacarbonyl and ethylene-acetylene mixtures were used as iron and carbon precursors. Highly dispersed nanoparticles, narrow size distributions and particles with about 3 to 20 nm mean sizes (in strong dependency with the experimental conditions) were obtained. Electron microscopy, X-ray diffraction and Raman spectroscopy are employed for structure and composition characterization of as-synthesized nanopowders.

2. Experimental

The Fe-C nanocomposites presented in this paper were synthesized by the laser co-pyrolysis of a gas-mixture, basically containing iron pentacarbonyl $Fe(CO)_5$ as iron precursor and a hydrocarbon mixture with ethylene-C_2H_4, and acetylene- C_2H_2. In all the experiments ethylene was used as carrier gas for iron pentacarbonyl vapours. Details of the experimental set-up were presented elsewhere [10, 11]. Essentially, the system is based on a cross-flow configuration. The reactant flow emerges in the reactor through a nozzle system where it is orthogonally intersected by the focused IR radiation beam. The laser induced pyrolysis reaction occurs into a small and well defined volume where usually a "flame"-illuminated zone appears. The confinement of gas precursors toward the flow axis and of the freshly nucleated particles is achieved by an external coaxial argon flow. The as synthetized particles are kept entrained by the gas stream and collected in a removable tank at the reaction cell exit before the vacuum pump. For each run, the flows and the pressure of the reactor were maintained constant using a mass flow controller systems and a downstream pressure controller (table 1).

The first aim was to establish the inlet geometry influence and for that we try two inlets. The first was a system with two concentric tubes where the central was design for

reactive premixed gases and the external for *Ar* flow. The second inlet had three concentric tubes: the central tube for iron precursor mixture (iron pentacarbonyl and ethylene), the intermediate one for carbon based precursor mixture (ethylene and acetylene) and the external tube for the *Ar* stream.

In all the experiments a CO_2 laser beam (about 70 Watt nominal power output, $\lambda =$ 10.6 μm) has been usually focused by a ZnSe cylindrical lens thus controlling the laser power density. For different rums, the laser intensity was varied by varying the dimensions of the focal spot.

For the experiments where the as synthesized particles seem to be instable at environmental conditions, the as synthesized Fe-C nanoparticles were slowly in-situ passivated according to a procedure described in details earlier [12].

The morphology and composition of the synthesized nanopowders were characterized by TEM, SAED, XRD and Raman spectroscopy. TEM micrographs of samples were recorded by using a CM 120 Philips 201 apparatus. Raman spectra were recorded using a Raman spectrometer TM 2001 Ocean Optics, 500 mW / 785 nn Solid State Diode (red laser system), 30 cm^{-1} resolution. For crystalline phase identification X-ray diffraction (XRD) was performed applying the JCPDS-files system. The samples were scanned from 20° to 85°. 2θ on a computer-controlled DRON DART UM2 diffractometer with a graphite monochromatized *CuKα* radiation in a step scan mode with a step width of 0.05^0 and an acquisition time on each step of 5s. The profile fitting calculation was performed using Voigt the crystallites sizes were calculated using the Debye-Scherrer formula.

3. Results and discussions

The specific laser pyrolysis processes involved in iron/ carbon cluster formation was already described in [15]. The set of experimental data presented in Table 1 was chosen based on some experimental observation. The first sign of reaction initiation is the flame, actually it is an illuminated zone where the laser beam crosses the reactive flow. A supplementary tool in experimental prediction is the IR analysis of exhaust gas. The ethylene decomposition is given by the depletion of its most intense absorption band centred at 950 cm^{-1}. By increasing the laser power density a fast effect should be iron pentacarbonyl decomposition, with iron nanoparticle formation accompanied by the apparition of CO absorption peaks in IR exhaust gases. Taking into account that the thermal decomposition process of iron pentacarbonil occurs al low temperatures, around 250 ^{0}C i.e. for low laser power density values just powder

formation and no visible flame may be observed. We exemplify this step with sample 3 (see table 1). After the synthesis this powder sample suffers a blind passivation/oxidation process.

At further increased laser power density the as synthesized iron nanoparticle catalyzes the hydrocarbon decomposition. In that case a visible flame exiting in the reaction zone is clearly seen. Maintaining the same hydrocarbon flows, pressure and laser power density constant, two parallel experiments were performed. In the first one, iron pentacarbonyl vapor was present in the reactive mixture leading to nanoparticle nucleation. In the second one, where just hydrocarbon mixture without iron precursor was present, no evidence of particle formation was observed (iron free carbon nanoparticle should be expected [13]). Furthermore, the IR exhaust gases spectra showed the absorption bands of CO from iron pentacarbonyl decomposition and depleted ethylene absorption peaks (as compared with non reacted mixture), while in the second case the IR gas spectra evidenced no reaction, i.e. the absorption maxima and their intensity are the same for the non reacted mixture and the mixture after laser irradiation. So we may assume that the carbon decomposition appears just in the presence of freshly formed iron cluster and most probable is a superficial carbon coating process. To sustain this assumption, analysis were perforated to evidence these predicted encapsulation features of the as synthesized powder (TEM, HREM). In earlier studies, the proper conditions for metallic iron core carbon encapsulation were established [11]. Thus process succeeded at higher laser power density than for iron cluster initiation. Sample 2 in Table 1 has approximately these parameters. Other important phenomenon is iron carburization, most probably by a diffusion process where carbon atoms penetrate through the iron core. When the laser power density was high enough, XRD and SAED analysis reveal iron carbides formation. This is exemplified by the main features of sample 1. Sample 4 (double- tubes inlet) was selected to show the influence of inlet geometry in comparison with sample 2, obtained at quasi the same experimental parameters (flows, gas ratio, pressure and laser power density). When exposed to air, the as synthesized nanoparticles were unstable, which means that parts of iron nanoparticles surface remain uncoated and consequently unprotected. The experiment was repeated and followed by the same passivation procedure as for sample 3 (more details for this process are found in [14]).

All collected iron-carbon nanoparticles are dark-brown to black inn color and they flow easily in air. When the powder is approached with a magnet, the particles are instantaneously attracted to it thus indicating that the nanoparticles are magnetic at room temperature. The specific laser pyrolysis processes involved in iron/carbon cluster formation was already described in [15]. In Table 1, the last column presents the mean particle

diameters. The TEM characterization of the Fe-C nanocomposites listed in Table 1 indicates that there are no basic differences between the particles dimensions but significant differences in shapes and internal structures (especially between S2 and S4).

Table I. Experimental parameters of the different production conditions discussed in thus article. During all experiments the Ar confinement flow was maintained at 1100 seem value.

sample	Tubes/ inlet	C_2H_4 carrier for $Fe(CO)_5$ (seem)	C_2H_4 in mixture (seem)	C_2H_2 in mixture (seem)	Pressure	Laser Power density (W/cm^2)	x_c (nm)
S1	3	50	30	50	500	2500	5.1
S2	3	50	30	50	500	2000	5.4
S3	3	50	30	50	500	1500	5.6
S4	2	50	30	50	500	2000	7.0

The samples Sl and S2 consist of nanometre-size particles (4-10 nm) showing to a higher or lower extent, the characteristic structure of encapsulated bodies. On the contrary, the samples S3 and S4 reveal the presence of particles with homogeneous structures sometimes different one from another. The particle size distribution is well fitted by a lognormal function and the mean size particle diameters (x_c- Table 1) were determined using this function. The medium resolution TEM image (Fig. 1) seems to indicate a rather even dispersion of *Fe* nanoparticles in a carbon matrix. Almost each particle presents a core (dark contrast) surrounded by a shell. The particle distribution indicates a mean size diameter of 7.0 nm for S4, a value which is significantly larger relatively to The S2 sample. One of the reasons should be a difference in the reaction mechanism, induced by the gas inlets geometry. Indeed, for sample S2, the residence time in the irradiated zone of iron pentacarbonyl vapors is significantly longer due to the direct proportionality of the flow speed with the inlet tube cross section.

The selected area electron diffraction patterns (SAED) (420 million magnifications) were obtained from an *80x80* nm area of particles lying on the grid. For all samples they reveal low dimension ordering (lack of bright spots and presence of diffuse diffraction rings). The SAED analysis of sample S1 (not presented here) exhibits well defined rings corresponding to 2.4 Å, 2.0 Å and 1.85 Å ascribed to Fe_3C -cohenite/cementite (JCPDS 35-0772) and no ring at 2.5 Å i.e. no evidence of gamma iron oxides. However, single SAED cannot discriminate metallic iron because its three important peaks are superposed with some relevant maxima of iron carbides. As an example the ring corresponding to 2.1-2.0 Å could be attributed both to (110) α-Fe plane and to (102), (220), (031) and (112) Fe_3C planes.

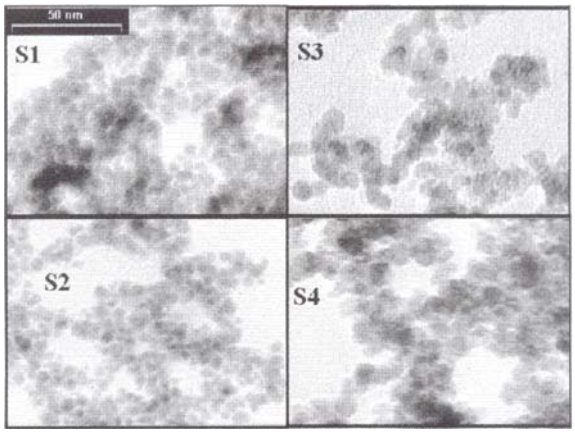

Fig. 1 Medium-resolution TEM images of the as-prepared samples

The SAED features of sample S2 (fig. 2 a) point to the presence of α-Fe (as identified by the diffraction rings corresponding to the (110), (200) and (112) planes), in spite of the diffraction maxima superposition of metallic iron and iron carbide phases, the iron carbide may be present in sample 2 as a minority phase, due to the lack of other important carbide rings, especially the one at 2.38 Å. Due to the weak-intensity ring at 2.5 Å, the presence of γ-Fe_2O_3/Fe_3O_4 may be not excluded and is probably due to a few particles not entirely encapsulated by carbon shell.

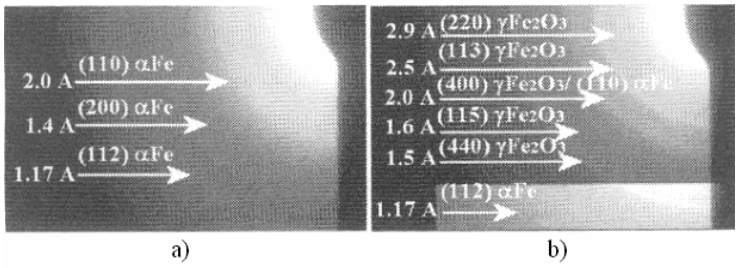

Fig. 2. SAED images for samples S2 (a) and S3 (b)

The SAED images for sample 3 shown in Fig. 2b seems to point out (the presence of γ-Fe_2O_3/Fe_3O_4 (identified by the most intense diffraction rings corresponding to the (113), (440) (220), (115) and (400) hkj planes) as a dominant crystalline phase. As fig 2b reveals, the ring corresponding to 2.0 – 2.1 Å has a higher intensity than the ring corresponding to 1.6 Å in spite of an inverse ratio between relative intensities of γ-Fe_2O_3, hkj planes: 33%, and 17% respectively. So the most probable interpretation for the 2.0 Å ring is a double contribution from γ-Fe_2O_3 - (400) plane and from α-Fe - (110) plane. Other argument for α-Fe presence is the very broad ring corresponding to 1.17 Å that appears when we enhance the lighting on SAED digitalized image (see the insert at the bottom of fig 2b). Assuming the presence of

carbides, even if the most important iron carbides have 100% diffraction maxima around 2.0 Å, some diffraction rings should also appear in the 2.4 - 2.2 Å region. Studying very carefully the corresponding zone on the digitalized SAED picture (including here the grey level diagram) no evidence of diffraction rings could be detected. Thus, the presence of iron carbides is improbable in this sample. The same criteria were used for the analysis of SAED image of sample S4 (not presented here). The grey level diagram of the digitalized image reveals the presence of a weak ring corresponding to 2.2 and 2.4 Å. SAED diagram could not discriminate between iron carbides, metallic iron or a mixture of both. However the dominant phase for sample S4 remains γ-Fe_2O_3. Other important information was obtained from X ray diffraction analysis (XRD) (see fig. 3).

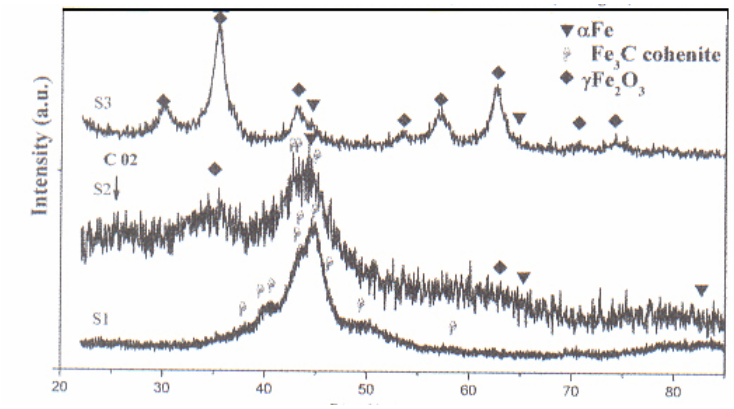

Fig. 3. XRD analysis for samples S1, S2, S3 and the identification of the main peaks

As general trend all XRD curves reveal a high amorphous feature (coming from an intense noise), most probably due to amorphous carbon. Furthermore XRD analysis reflects an important dependency, of particle chemical structure with laser power density. At high radiation densities iron carbides are present (sample S1), at medium values metallic iron is the dominant phase (sample S2) and at lower laser power γ-Fe_2O_3, is the principal phase (however the oxide phase appears after the passivation procedure, many of the as synthesized powers being most probably uncovered iron nanoparticles) (sample S3). The S1 XRD pattern shows the presence of Fe_3C (JCPDS file: 35-0772) as dominant phase. The metallic iron or other carbides could not be excluded. Due to this incertitude we were obliged to make supplementary analysis for this sample and the most relevant was the Mossbauer Spectroscopy. First analysis made at room temperature reveals an entire superparamagnetic character, due to the very fine (less then 10 nm) magnetic structures. The Mossbauer spectrum at 23 K allows the identification of a dominant Fe_3C sextets (76% at. Fe), accompanied by α-Fe sextets (13% at. Fe), γ-Fe doublets

(2% at. Fe) and γ-Fe_2O_3/Fe_3O_4 sextets (9 at. %). Due to the small quantity, and very small crystalline domain of oxides phase it is still difficult to make separation between these two iron oxide phases even at 23 K.

The S2 XRD pattern exhibits two very broad peaks revealing very small crystallite dimensions (less than 4 nm). The peak centered at 35.7 ^{0} could be attributed to (311) γ-Fe_2O_3 and represents the most intense diffraction maximum. Both *αFe* and iron carbides (Fe3C. Fe5C2 and Fe7C3) have the most intense diffractions in the 42 - 45 ^{0} region but carbides phases have significant peaks also in the 37- 41 ^{0} domain. Therefore the second broad peak around 44.7 ^{0} could be ascribed to metallic iron phase and due to the lack of other peaks in the 37-41 ^{0} region just to small amounts of iron carbides. Also the very broad and less intense peak at about 25.5 ^{0} indicate that the carbon is not completely amorphous as for the other two samples.

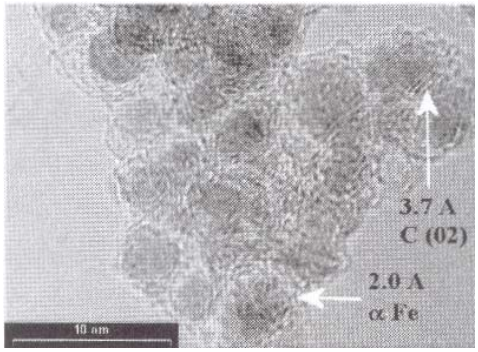

Fig. 4. HRRM image for sample S2

The XRD spectrum of sample S4 (not presented here) shows very broad peaks that may ascertain a dominant γ-Fe_2O_3-Fe_3O_4, phase quite similar to sample S3 (same cell parameter). The iron carbide phase is presented as secondary phase in this sample and seems to be a mixture of the both Fe_3C phases (JCPDS files 34-0001 and 35-0772) as their relative intensities are endorsed. However, due to the very low crystallites sizes and poor crystallinity, the ill-defined profile makes hard to discriminate between these phases and the possible presence of traces of others iron carbide or metallic iron phases. In the HREM image for sample S2 displayed in Fig. 4 one may notice the difference between the structure of the rather spherical core, having quasi-monocrystalline structure and the outside layers. For sample 2 the identified interplanar distance (2.0 Å) of the core is closed to (110) α-Fe values. Monatomic shells are covering the iron core: with inter shell distances of 3.7 Å that could be assumed as carbon turbostratic planes. An interplanar distance value that is somewhat larger than for crystalline graphite (3.35 Å for (002) plane) is quite often encountered in case of nanosized pyrolytic carbon and seems to be an effect of the reduced number of stacking layers [13].

Raman spectroscopy was used in order to monitor the carbon content and different processes evolving in samples through the oxidation/carburization processes. In almost all cases, carbon presented amorphous features Specific Roman shifts for 2 superposed samples are displayed in Fig 5: S2 - for Fe core encapsulated in carbon shell nauoparticles and S4 - for basically iron oxidized nanoparticles. The S2 displayed spectrum reveals a high carbon content with rather characteristic D and G bands of amorphous carbon (at 1355 cm^{-1} and 1584 cm^{-1}, respectively). Probably due to its amorphous character and/or low content, XRD and SAED analysis of all samples seems to not indicate graphitic like-carbon presence. In contrast, the Raman spectrum of sample S4 shows a strong oxidative feature represented by γ-Fe_2O_3 [16], due to a blind and superficial oxidation process that the as synthesized iron nanoparticles undergo. In this sample a minor contribution for amorphous carbon (D and G bands) also appears.

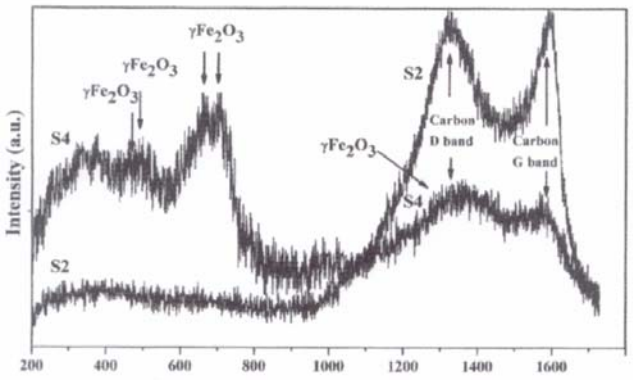

Raman shift [cm^{-1}]

Fig. 5 Raman spectra of two different iron based nanopowders: sample S2 and sample S4

4. Conclusions

Different iron carbon nanostructures have been obtained using the laser pyrolysis of iron pentacarbonyI vapour, ethylene and acetylene based mixtures. Using an inlet with 3 tubes, iron or iron carbide core with carbon shells have been obtained. The iron based phase depends on laser power density: metallic iron at medium values (2000 W/cm^2) and cohenite (Fe_3C) at higher values. At lower laser power density, the iron nanoparticles were not entirely coated by carbon shells and an almost entirely oxidative transformation appears, Fe_3C/ α- Fe/ γ-Fe_2O_3 /Fe_3O_4 nanoparticles with out encapsulation features have been obtained in case of double-tube gas inlet geometry.

References

[1] L. Si, D. Zhang, D. Y. Gcng, C. Y. You, X. G. Zhao, W. S. Zhang, Carbon 41, (2003) 247

[2] X. L. Dong, Z. D. Zhang, Y. C. Chuang, S. R. Jin, J. Ippl. Plrys., 86 (1999) 6701

[3] X. W. Wu, H. Zhoua, R. J. M. van de Veerdonk, T. J. Klennmer, C. Liu, N. Shukla, D. Weller, M. Tanase, D. E. Laughlin, J. Appl. Phys., 93, (2003) 7181

[4] J. P. Hare, W. K Hsu, H.W. Kroto, A. Lappas, K. Prassides, M. Terrones, D. R. M. Walton, Chem. Mater, 8, (1996) 6

[5] X. L. Dong, Z. D. Zhang, Q. F. Xiao, X. G. Zhao, Y. C. Chuang, S. R. Jin, W. M. Sun, Z.

[6] J. Li, Z. X. Zheng, H. Yang, Journal Of Materials Science, 33, (1998) 1915

F. Huisken, B. Kohn, R. Alexandrescu, 1. Morjan, J. Chem. Phys., 113, (2000) 6579

[7] M. P. Morales. S Veintemillas-Verdaguer, M. I. Montero, C. J. Serna, A. Roig, L. L. Casas, B. Martinez, F. Sandiumenge, Chemistry of Materials, 11 (1999) 3058

[8] I. Morjan, R. Alexandrescu, I. Soare, F. Durnitrache, 1. Sandu, 1. Voicu, A. Crunteanu, E. Vasile, V. Ciupina, S. Martelli, Mater. Sci. Eng., C, 1020 (2002) 1

[9] R. Alexandrescu, S. Cojocaru, A. Crunteanu, 1. Morjan, 1. Voicu, L. Diamandescu, F. Vasiliu, F. Huisken, B. Kohn, J. Phys. IV, 9 Pr8, (1999) 537

[10] S. 1. Nikitenko, Y. Koltypin, O. Palchik, 1. Felner, X. N. Xu, A. Gedanken, Angewandte Chemie Int. Ed., 40, (2001) 4447

[11] F. Dumitrache, l. Morjan, R. Alexandrescu, B. Rand, V. Ciupina, G. Prodan, 1. Voicu, 1. Sandu, 1. Soare, M. Ploscaru, C. Fleaca, R. Brydson, R. E. Vasile, "Iron-carbon nanocomposite obt. by l. ind. gas-phase reactions", Proc. of SPIE, 4977, (2003) 670-680

[12] F. Dumitrache, V Ciupina, I. Morjan, R. Alexandrescu, 1. Voicu, I. Soare, L. Albu, R. E. Morjan, F. M. Savoiu, G. Prodan, Proc. of SPIE, 2003 (will be published)

[13] A Galvez, N. Herlin-Boime, et all, Carbon, 40,(2002)2775

[14] F. Dumitrache, 1. Morjan, R. Alexandrescu, V. Ciupina, G. Prodan, 1. Voicu, C. Fleaca, L. Albu, M. Savoiu, 1. Sandu, E. Popovici, 1. Soare, Appl. Surf. Sci., 247, (2005) 25

[15] R. Alexandrescu. 1. Morjan, F. Dumitrache, l. Voicu, 1. Soare, 1. Sandu, C.T. Fleaca, Solid State Phenomena, 99- 100, (2004) 181

[16] J. C. Rubim, M. H. Sousa, J. C. O. Silva, F. A. Tourinho, Braz. J. of Physics, 31, (2000) 402